Analysis of Random Nonuniform Transmission Line Response under Plane-Wave Illumination with a Perturbation Decomposition-Polynomial Chaos Expansion Method

Jinpeng Yang, Xiaoying Sun, Yu Zhao, Jian Chen, and Hanqing Wang

College of Communication Engineering
Jilin University, Chang Chun, 130012, China
yangjp15@mails.jlu.edu.cn, sunxy@jlu.edu.cn, yzhao@jlu.edu.cn,
chenjian@jlu.edu.cn, hqwang16@mails.jlu.edu.cn

Abstract ─ A perturbation decomposition-polynomial chaos expansion method is presented to evaluate the electromagnetic effects of random nonuniform transmission line under plane-wave illumination. The nonuniformity is represented as perturbation with respect to the reference uniform transmission line. Moreover, by expanding the unknown random parameters in terms of orthogonal polynomials, the stochastic transmission line equation is projected into a set of deterministic transmission line equations. Numerical simulations are presented for several typical deterministic and random nonuniform transmission lines above an ideal ground. The results show that the proposed perturbation decomposition-polynomial chaos expansion method is accurate and computationally efficient compared with the traditional uniform cascaded section method and Monte Carlo method.

Index Terms ─ Deterministic nonuniform transmission line, parameter uncertainty, perturbation decomposition, plane-wave illumination, polynomial chaos expansion, random nonuniform transmission line.

I. INTRODUCTION

Cables and wires are usually the most sensitive parts in the electromagnetic compatibility problems of electrical and electronic systems. Owing to the mechanical manufacturing tolerances or manual installation manner errors, uncertainty [1,2] and nonuniformity [3-8] of transmission line (TL) are often encountered in practical applications, such as linearly tapered micro-strip line [3], interconnects subject to line-edge roughness [4], twisted pair [5], and undesired asymmetry differential lines [6], which may significantly affect the signal integrity and immunity. The intentional/unintentional electromagnetic interference in the free space may also aggravate the distortion effect. Therefore, it is of great significance to analyze the effect of randomness and nonuniformity on the response of TL under plane-wave illumination.

Transmission line theory [9] has been investigated for a long time. For a deterministic uniform transmission line (DUTL), the coupling mechanism is well established and has been overviewed in [10,11]. For a random uniform transmission line (RUTL), several methods have been proposed [12-16]. A direct method is the Monte Carlo (MC) method [12,13], which collects statistical information through huge samplings of random parameters to perform extensive repeated simulations of deterministic models. Although robust, MC has a large computational load. Another approach called the polynomial chaos expansion (PCE) method [14-16], which describes the statistical behavior through the orthogonal basis of a series of random variables, is fairly accurate and much faster than the MC method.

For a deterministic nonuniform transmission line (DNTL), the conventional approach is the uniform cascaded section (UCS) method [9]. UCS tackles the nonuniformity problem by subdividing the DNTL into large local uniform sections [17-21], thus leading to long computation time. Recently, a computationally efficient method called the equivalent source method [22] has been proposed to cope with DNTL. Subsequently, it has been extended to the perturbation decomposition technique (PDT) to cope with the crosstalk problem of different types of DNTL [3-8]. However, studies on the electromagnetic effect of random nonuniform transmission lines (RNTL) are scant. Moreover, the PDT is limited to DNTL, and cannot be directly applied to RNTL. So far, the PDT has only been applied to the crosstalk problems, and the ability of coping with DNTL under plane-wave illumination has not been verified.

Therefore, an N^{th}-order perturbation decomposition-M^{th}-order polynomial chaos expansion method ((N^{th}, M^{th})-order PD-PCE) is presented to analyze the RNTL response under external plane-wave illumination in this paper. The nonuniformity of TL is modeled as an equivalent distribution source for the reference uniform transmission line. Subsequently, based on the orthogonal

Submitted On: December 3, 2017
Accepted On: December 24, 2018

polynomial expansion of unknown random parameters, the stochastic transmission line equation is projected into a set of deterministic transmission line equations through a stochastic Galerkin method.

The rest of this paper is structured as follows. The derivation of the PD-PCE method is demonstrated in Section II. In Section III, the feasibility and strength of the PD-PCE method are validated by applying it to several typical simplifying RNTLs. Finally, a summary is given in Section IV.

II. PERTURBATION DECOMPOSITION-POLYNOMIAL CHAOS EXPANSION METHOD

In this section, the general solution of RNTL under plane-wave illumination is derived. Four cases of RNTL commonly observed in practical applications are considered, including vibrating RNTL, as shown in Figs. 1 (a)–(b), and floating RNTL, as shown in Figs. 1 (c)–(d). The radius of the four cases of RNTL is r_a. The left and right ends of RNTL are terminated with the impedances Z_L and Z_R, respectively. The heights of the four cases of RNTL are defined as follows:

$$\begin{aligned} h(z,\varepsilon) &= H_1 + 2\cdot(\delta_h\cdot\varepsilon)\cdot z/L && : \text{case } a,\\ h(z,\varepsilon) &= (H_2 - H_1 - \delta_h\cdot\varepsilon)\cdot(2\cdot z/L)^2 + H_1 + \delta_h\cdot\varepsilon && : \text{case } b,\\ h(z,\varepsilon) &= H_1 + \delta_h\cdot\varepsilon + 2\cdot(H_2 - H_1)\cdot z/L && : \text{case } c,\\ h(z,\varepsilon) &= (H_2 - H_1)\cdot(2\cdot z/L)^2 + H_1 + \delta_h\cdot\varepsilon && : \text{case } d, \end{aligned} \tag{1}$$

where $z\in[-L/2, L/2]$, L is the length of the RNTL in the z direction. H_1 is the height of the RNTL at $z=0$, H_2 is the height of the RNTL at $z=L/2$, ε is the normalized random variable, which is assumed to be uniformly distributed in [-1,1]. δ_h is the uncertainty coefficient.

In particular, for case c and case d, the RNTL becomes DNTL when $\delta_h = 0$ and $H_1 \neq H_2$, and the RNTL becomes RUTL when $\delta_h \neq 0$ and $H_1 = H_2$. Both DNTL and RUTL are special cases of RNTL.

There are two main steps for the construction of the proposed (N^{th}, P^{th})-order PD-PCE method for RNTL. In the first step, the perturbation solution for the RNTL under plane-wave illumination is derived; therefore, the RNTL equation is converted to an RUTL equation. In the second step, the RUTL equation is converted to a DUTL equation by applying the polynomial chaos theory.

A. Plane wave parameters

As shown in Fig. 2, considering an incident plane-wave electric field $\vec{E}^{inc}$ with amplitude E_0 described by:

$$\vec{E}^{inc} = E_0\left(e_x\vec{x} + e_y\vec{y} + e_z\vec{z}\right)e^{-j\vec{k}\cdot\vec{r}}, \tag{2}$$

where $\vec{r}$ is the observation position vector, and the scalar components e_x, e_y, and e_z in the direction of unit vectors $\hat{x}$, $\hat{y}$, and $\hat{z}$, respectively, are defined as:

$$\begin{aligned} e_x &= \cos\alpha\cos\theta\cos\varphi - \sin\alpha\sin\varphi,\\ e_y &= \cos\alpha\cos\theta\sin\varphi + \sin\alpha\cos\varphi,\\ e_z &= -\cos\alpha\sin\theta, \end{aligned} \tag{3}$$

where α is the polarization angle, θ is the elevation angle, and φ is the azimuth angle. The wave vector $\vec{k}$ with free space wave number k_0 is defined as:

$$\begin{aligned} \vec{k} &= k_x\hat{x} + k_y\hat{y} + k_z\hat{z}\\ &= k_0\sin\theta\cos\varphi\hat{x} + k_0\sin\theta\sin\varphi\hat{y} + k_0\cos\theta\hat{z}, \end{aligned} \tag{4}$$

where k_x, k_y, and k_z are the components of the wave vector along the unit vectors $\hat{x}$, $\hat{y}$, and $\hat{z}$, respectively.

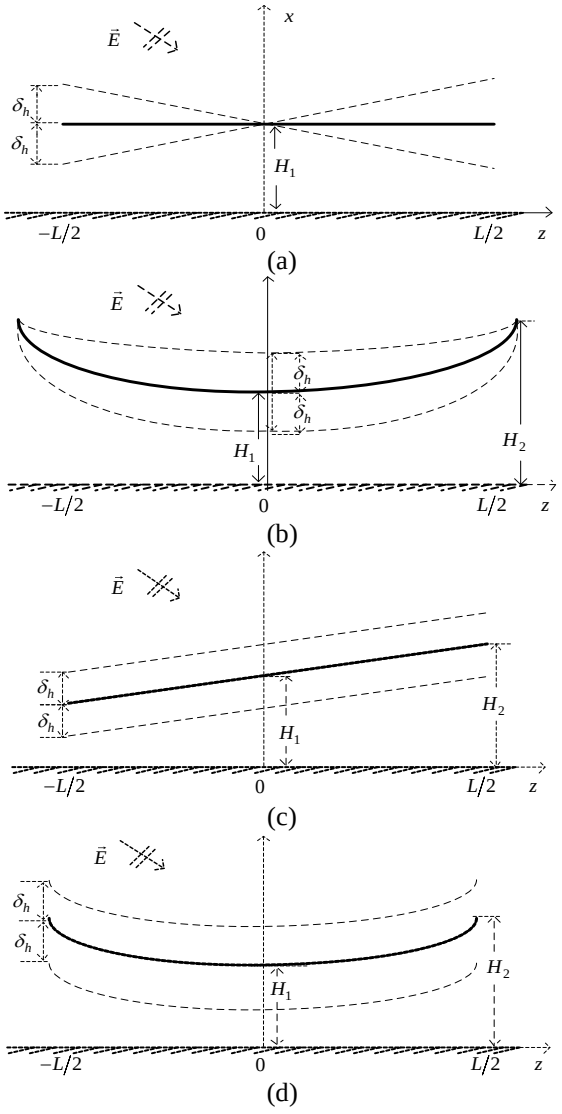

Fig. 1. (a) Case *a*: Random vibrating nonuniform straight transmission line. (b) Case *b*: Random vibrating nonuniform bending transmission line. (c) Case *c*: Random floating nonuniform straight transmission line. (d) Case *d*: Random floating nonuniform bending transmission line.

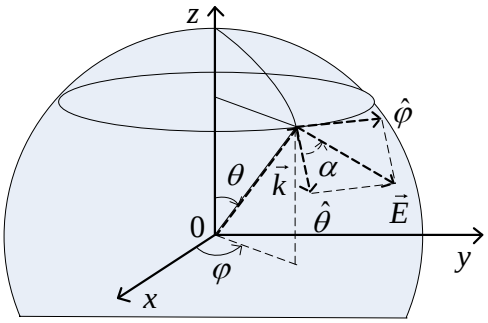

Fig. 2. Plane-wave incident direction.

Considering the reflection effect of ground, total electric field is the sum of the incident and reflection fields, and the *z* component $E_z^{tot}(z,\varepsilon)$ and *x* component $E_x^{tot}(z,\varepsilon)$ of the total electric field are given as follows:

$$\begin{aligned} E_z^{tot}(z,\varepsilon) &= -2jE_0 e_z \sin\left(k_x h(z,\varepsilon)\right) e^{-j\left(k_y y + k_z z\right)}, \\ E_x^{tot}(z,\varepsilon) &= \ \ 2E_0 e_x \cos\left(k_x h(z,\varepsilon)\right) e^{-j\left(k_y y + k_z z\right)}. \end{aligned} \tag{5}$$

B. Perturbation decomposition of random nonuniform transmission line equation

The Agrawal formula [11], which describes field-to-line coupling for an RNTL, is given by:

$$\begin{aligned} &\frac{d}{dz}V^s(z,\varepsilon) + j\omega L(z,\varepsilon) I(z,\varepsilon) = V_F^{'}(z,\varepsilon), \\ &\frac{d}{dz}I(z,\varepsilon) + j\omega C(z,\varepsilon) V^s(z,\varepsilon) = 0, \end{aligned} \tag{6}$$

where $V^s(z,\varepsilon)$ and $I(z,\varepsilon)$ define the random scattering voltage and current of RNTL, respectively. $L(z,\varepsilon)$ and $C(z,\varepsilon)$ are the per unit length (p.u.l.) random inductance and capacitance of the RNTL, respectively. The distributed voltage source $V_F^{'}(z,\varepsilon)$ is defined as:

$$V_F^{'}(z,\varepsilon) = E_z^{tot}(z,\varepsilon)\cdot\cos\left(\eta(z,\varepsilon)\right) + E_x^{tot}(z,\varepsilon)\cdot\sin\left(\eta(z,\varepsilon)\right), \tag{7}$$

where $\eta(z,\varepsilon)$ is the position-dependent random inclination angle of the RNTL. The total voltage of the RNTL is defined as:

$$V(z,\varepsilon) = V^s(z,\varepsilon) - V^{ex}(z,\varepsilon), \tag{8}$$

where the excitation voltage $\boldsymbol{V}^{ex}(z,\varepsilon)$ is defined as:

$$V^{ex}(z,\varepsilon) = \int_0^{h(z,\varepsilon)} E_x^{tot}(z,\varepsilon)dx. \tag{9}$$

To deal with the nonuniform problem of the TL, the perturbation decomposition technique [5] is applied to the scattering voltage, current, capacitance, and inductance as follows:

$$\begin{aligned} V^s(z,\varepsilon) &\approx V_0^s(z,\varepsilon) + V_1^s(z,\varepsilon) + \ldots + V_N^s(z,\varepsilon), \\ I(z,\varepsilon) &\approx I_0(z,\varepsilon) + I_1(z,\varepsilon) + \ldots + I_N(z,\varepsilon), \\ C(z,\varepsilon) &= C_0(\varepsilon) + C_1(z,\varepsilon), \\ L(z,\varepsilon) &= L_0(\varepsilon) + L_1(z,\varepsilon), \end{aligned} \tag{10}$$

where V_0^s and I_0 are the 0th-order perturbation random scattering voltage and current, respectively. V_n^s and I_n $(n=1,2,...,N)$ are the *n*th-order perturbation random scattering voltage and current, respectively. *N* is the truncated order. C_0 (C_1) and L_0 (L_1) are the 0th-order (1st-order) perturbation p.u.l. random capacitance and inductance, respectively.

Substituting equation (10) into equation (6), the RNTL equation can be decomposed to 0th-order and *n*th-order $(n=1,2,...,N)$ RUTL equations, as follows:

$$\begin{aligned} &\frac{d}{dz}V_0^s(z,\varepsilon) + j\omega L_0(\varepsilon) I_0(z,\varepsilon) = V_F^{'}(z,\varepsilon), \\ &\frac{d}{dz}I_0(z,\varepsilon) + j\omega C_0(\varepsilon) V_0^s(z,\varepsilon) = 0, \end{aligned} \tag{11}$$

$$\begin{aligned} &\frac{d}{dz}V_n^s(z,\varepsilon) + j\omega L_0(\varepsilon) I_n(z,\varepsilon) = -j\omega L_1(z,\varepsilon) I_{n-1}(z,\varepsilon), \\ &\frac{d}{dz}I_n(z,\varepsilon) + j\omega C_0(\varepsilon) V_n^s(z,\varepsilon) = -j\omega C_1(z,\varepsilon) V_{n-1}^s(z,\varepsilon). \end{aligned} \tag{12}$$

For the 0th-order perturbation equation (11), the excitation term directly originates from the incident plane-wave. For the *n*th-order perturbation equation (12), the excitation terms originate from the (*n*-1)th-order perturbation scattering voltage and current.

C. Polynomial chaos expansion

To solve the RUTL equations (11) and (12), the PCE method [14] was adopted to expand the random variable in equations (11) and (12) as follows:

$$\begin{aligned} &V_0^s(z,\varepsilon) = \sum_{p=0}^{P} V_0^{s,p}(z)\cdot\phi_p(\varepsilon), V_n^s(z,\varepsilon) = \sum_{p=0}^{P} V_n^{s,p}(z)\cdot\phi_p(\varepsilon), \\ &I_0(z,\varepsilon) = \sum_{p=0}^{P} I_0^p(z)\cdot\phi_p(\varepsilon),\ I_n(z,\varepsilon) = \sum_{p=0}^{P} I_n^p(z)\cdot\phi_p(\varepsilon), \\ &V_F^{'}(z,\varepsilon) = \sum_{p=0}^{P} V_F^{p'}(z)\cdot\phi_p(\varepsilon), \end{aligned} \tag{13a}$$

$$\begin{aligned} &C_0(\varepsilon) = \sum_{p=0}^{P} C_0^p\cdot\phi_p(\varepsilon), C_1(z,\varepsilon) = \sum_{p=0}^{P} C_1^p(z)\cdot\phi_p(\varepsilon), \\ &L_0(\varepsilon) = \sum_{p=0}^{P} L_0^p\cdot\phi_p(\varepsilon),\ L_1(z,\varepsilon) = \sum_{p=0}^{P} L_1^p(z)\cdot\phi_p(\varepsilon), \end{aligned} \tag{13b}$$

where $V_0^{s,p}$ $(V_n^{s,p})$ and I_0^p (I_n^p) represent the (0^{th}, p^{th})-order ((n^{th}, p^{th})-order) PD-PCE coefficients for scattering voltage and current, respectively. $V_F^{p'}$ represents the p^{th}-order PCE coefficients for the distributed voltage source. C_0^p (C_1^p) and L_0^p (L_1^p) represent the (0^{th}, p^{th})-order ((1^{st}, p^{th})-order) PD-PCE coefficients for p.u.l. capacitance and inductance, respectively. $\phi_p(\varepsilon)$ is a p^{th}-order polynomial. The random variable is assumed to be uniformly distributed; hence, the Legendre orthogonal polynomials are appropriate for this case [14], as shown in Table 1. For the random variables of number *q* and order *m*, the total number of expansion items is $(P+1)!=(p+q)!/(p!q!)$. In this study, there is only one random variable; hence, q=1.

Table 1: Legendre polynomial for one random variable

Order *p*	**p^{th}-order polynomial** ϕ_p	$\langle \phi_p, \phi_p \rangle$
0	1	1
1	ε	1/3
2	$\left(3\varepsilon^2 - 1\right)/2$	1/5
…	…	…
p	$\frac{1}{2^p\, p!}\frac{\partial}{\partial \varepsilon^p}\left(\varepsilon^2 - 1\right)^p$	$1/(2p+1)$

Substituting equation (13) into (11), the original 0th-order perturbation RUTL equation is expanded as:

$$\frac{d}{dz}\sum_{p=0}^{P_0} V_0^{s,p}(z)\phi_p(\varepsilon) + j\omega\sum_{t=0}^{P_T} L_0^t\phi_t(\varepsilon)\sum_{p=0}^{P_0} I_0^p(z)\phi_p(\varepsilon) = \sum_{p=0}^{P_0} V_F^{p'}(z)\,\phi_p(\varepsilon), \quad (14)$$

$$\frac{d}{dz}\sum_{p=0}^{P_0} I_0^p(z)\phi_p(\varepsilon) + j\omega\sum_{t=0}^{P_T} C_0^t\phi_t(\varepsilon)\sum_{p=0}^{P_0} V_0^{s,p}(z)\phi_p(\varepsilon) = 0,$$

where P_0 and P_T are the expansion orders. Through a stochastic Galerkin method, equation (14) was projected to the Legendre orthogonal basis as follows:

$$\frac{d}{dz}\sum_{p=0}^{P_0} V_0^{s,p}(z)\langle\phi_p(\varepsilon),\phi_k(\varepsilon)\rangle + j\omega\sum_{t=0}^{P_T}\sum_{p=0}^{P_0} L_0^t I_0^p(z)\langle\phi_t(\varepsilon)\phi_p(\varepsilon),\phi_k(\varepsilon)\rangle = \sum_{p=0}^{P_0} V_F^{p'}(z)\,\langle\phi_p(\varepsilon),\phi_k(\varepsilon)\rangle, \quad (15)$$

$$\frac{d}{dz}\sum_{p=0}^{P_0} I_0^p(z)\langle\phi_p(\varepsilon),\phi_k(\varepsilon)\rangle + j\omega\sum_{t=0}^{P_T}\sum_{p=0}^{P_0} C_0^t V_0^{s,p}(z)\langle\phi_t(\varepsilon)\phi_p(\varepsilon),\phi_k(\varepsilon)\rangle = 0.$$

The symbol $\langle\ ,\ \rangle$ represents the inner product over the definition domain of the random variable. Solving (15), the following 0th-order perturbation augmented equation in matrix form can be obtained.

$$\frac{d}{dz}\begin{bmatrix}\boldsymbol{V}_0^s(z)\\ \boldsymbol{I}_0(z)\end{bmatrix} + \begin{bmatrix}\boldsymbol{0} & j\omega\boldsymbol{L}_0\\ j\omega\boldsymbol{C}_0 & \boldsymbol{0}\end{bmatrix}\begin{bmatrix}\boldsymbol{V}_0^s(z)\\ \boldsymbol{I}_0(z)\end{bmatrix} = \begin{bmatrix}\boldsymbol{V}_F^{'}(z)\\ \boldsymbol{0}\end{bmatrix}, \quad (16)$$

where $\boldsymbol{V}_0^s(z)$ and $\boldsymbol{I}_0(z)$ are the 0th-order perturbation $(P_0+1)\times 1$ scattering voltage and current vector, respectively. $\boldsymbol{V}_F^{'}(z)$ is the 0th-order $(P_0+1)\times 1$ distributed voltage source vector. $\boldsymbol{L}_0$ and $\boldsymbol{C}_0$ are the 0th-order perturbation $(P_0+1)\times(P_0+1)$ inductance and capacitance matrix, respectively. The i^{th} row and j^{th} column $(i, j = 1,2,...,P_0+1)$ of $\boldsymbol{L}_0$ and $\boldsymbol{C}_0$ are given as follows:

$$\boldsymbol{L}_0\big|_{ij} = \sum_{p=0}^{P_0} L_0^p\alpha_{pji}, \boldsymbol{C}_0\big|_{ij} = \sum_{p=0}^{P_0} C_0^p\alpha_{pji}, \quad (17)$$

where,

$$\alpha_{pji} = \langle\phi_p\phi_j,\phi_i\rangle/\langle\phi_i,\phi_i\rangle. \quad (18)$$

Similarly, substituting equation (13) into (12), the original n^{th}-order perturbation RUTL equation becomes:

$$\begin{aligned}\frac{d}{dz}\sum_{p=0}^{P_n} V_n^{s,p}(z)\phi_p(\varepsilon) + j\omega\sum_{t=0}^{P_T} L_0^t\phi_t(\varepsilon)\sum_{p=0}^{P_n} I_n^p(z)\phi_p(\varepsilon) &= -j\omega\sum_{t=0}^{P_T} L_1^t(z)\phi_t(\varepsilon)\sum_{p=0}^{P_{n-1}} I_{n-1}^p(z)\phi_p(\varepsilon),\\ \frac{d}{dz}\sum_{p=0}^{P_n} I_n^p(z)\phi_p(\varepsilon) + j\omega\sum_{t=0}^{P_T} C_0^t\phi_t(\varepsilon)\sum_{p=0}^{P_n} V_n^{s,p}(z)\phi_p(\varepsilon) &= -j\omega\sum_{t=0}^{P_T} C_1^t(z)\phi_t(\varepsilon)\sum_{p=0}^{P_{n-1}} V_{n-1}^{s,p}(z)\phi_p(\varepsilon),\end{aligned} \quad (19)$$

where $P_n = P_T + P_{n-1}$ $(n = 1,2,...,N)$. Projecting equation (19) to the Legendre orthogonal basis, the following equations can be obtained:

$$\begin{aligned}\frac{d}{dz}\sum_{p=0}^{P_n} V_n^{s,p}(z)\langle\phi_p(\varepsilon),\phi_k(\varepsilon)\rangle + j\omega\sum_{t=0}^{P_T}\sum_{p=0}^{P_n} L_0^t I_n^p(z)\langle\phi_t(\varepsilon)\phi_p(\varepsilon),\phi_k(\varepsilon)\rangle &= -j\omega\sum_{t=0}^{P_T}\sum_{p=0}^{P_{n-1}} L_1^t(z) I_{n-1}^p(z)\langle\phi_t(\varepsilon)\phi_p(\varepsilon),\phi_k(\varepsilon)\rangle,\\ \frac{d}{dz}\sum_{p=0}^{P_n} I_n^p(z)\langle\phi_p(\varepsilon),\phi_k(\varepsilon)\rangle + j\omega\sum_{t=0}^{P_T}\sum_{p=0}^{P_n} C_0^t V_n^{s,p}(z)\langle\phi_t(\varepsilon)\phi_p(\varepsilon),\phi_k(\varepsilon)\rangle &= -j\omega\sum_{t=0}^{P_T}\sum_{p=0}^{P_{n-1}} C_1^t(z) V_{n-1}^{s,p}(z)\langle\phi_t(\varepsilon)\phi_p(\varepsilon),\phi_k(\varepsilon)\rangle.\end{aligned} \quad (20)$$

Solving (20), the n^{th}-order perturbation augmented equation in matrix form can be obtained as follows:

$$\frac{d}{dz}\begin{bmatrix}\boldsymbol{V}_n^s(z)\\ \boldsymbol{I}_n(z)\end{bmatrix} + \begin{bmatrix}\boldsymbol{0} & j\omega\boldsymbol{L}_0\\ j\omega\boldsymbol{C}_0 & \boldsymbol{0}\end{bmatrix}\begin{bmatrix}\boldsymbol{V}_n^s(z)\\ \boldsymbol{I}_n(z)\end{bmatrix} = \begin{bmatrix}\boldsymbol{V}_F^{n'}(z)\\ \boldsymbol{I}_F^{n'}(z)\end{bmatrix}, \quad (21)$$

where the n^{th}-order distributed voltage source vector $\boldsymbol{V}_F^{n'}(z)$ and the distributed current source vector $\boldsymbol{I}_F^{n'}(z)$ are:

$$\begin{bmatrix}\boldsymbol{V}_F^{n'}(z)\\ \boldsymbol{I}_F^{n'}(z)\end{bmatrix} = -\begin{bmatrix}\boldsymbol{0} & j\omega\boldsymbol{L}_1\\ j\omega\boldsymbol{C}_1 & \boldsymbol{0}\end{bmatrix}\begin{bmatrix}\boldsymbol{V}_{n-1}^s(z)\\ \boldsymbol{I}_{n-1}(z)\end{bmatrix}, \quad (22)$$

where $\boldsymbol{L}_1$ and $\boldsymbol{C}_1$ are the 1st-order perturbation $(P_{n-1}+1)\times(P_{n-1}+1)$ inductance and capacitance matrix, respectively. The i^{th} row and j^{th} column $(i, j = 1,2,...,P_n+1)$ of $\boldsymbol{L}_1$ and $\boldsymbol{C}_1$ are given as follows:

$$\boldsymbol{L}_1\big|_{ij} = \sum_{p=0}^{P_{n-1}} L_1^p\alpha_{pji}, \boldsymbol{C}_1\big|_{ij} = \sum_{p=0}^{P_{n-1}} C_1^p\alpha_{pji}. \quad (23)$$

D. Modal decomposition

As $\boldsymbol{L}_0$ and $\boldsymbol{C}_0$ are full matrixes, the scattering voltage and current vector in (16) are coupled. The similarity transformation method [9] is used to decouple equation (16). Through voltage (current) transformation matrix $\boldsymbol{T}_V$ ($\boldsymbol{T}_I$), the voltage vector $\boldsymbol{V}_0^s$ and current vector $\boldsymbol{I}_0$ were cast into modal voltage vector $\boldsymbol{V}_{m,0}^s$ and modal current vector $\boldsymbol{I}_{m,0}$ as follows:

$$\begin{bmatrix}\boldsymbol{V}_0^s(z)\\ \boldsymbol{I}_0(z)\end{bmatrix} = \begin{bmatrix}\boldsymbol{T}_V & \boldsymbol{0}\\ \boldsymbol{0} & \boldsymbol{T}_I\end{bmatrix}\begin{bmatrix}\boldsymbol{V}_{m,0}^s(z)\\ \boldsymbol{I}_{m,0}(z)\end{bmatrix}. \quad (24)$$

Substituting equation (24) into equation (16), the

following 0th-order perturbation decoupled modal TL equation can be obtained:

$$\frac{d}{dz}\begin{bmatrix}\boldsymbol{V}_{m,0}^{s}(z)\\ \boldsymbol{I}_{m,0}(z)\end{bmatrix}+\begin{bmatrix}\boldsymbol{0} & j\omega\boldsymbol{L}_{m,0}\\ j\omega\boldsymbol{C}_{m,0} & \boldsymbol{0}\end{bmatrix}\begin{bmatrix}\boldsymbol{V}_{m,0}^{s}(z)\\ \boldsymbol{I}_{m,0}(z)\end{bmatrix}=\begin{bmatrix}\boldsymbol{V}_{Fm}^{'}(z)\\ \boldsymbol{0}\end{bmatrix}, \quad (25)$$

where $\boldsymbol{L}_{m,0}$ and $\boldsymbol{C}_{m,0}$ can be obtained by:

$$\boldsymbol{L}_{m,0}=\boldsymbol{T}_V^{-1}\boldsymbol{L}_0\boldsymbol{T}_I,\ \boldsymbol{C}_{m,0}=\boldsymbol{T}_I^{-1}\boldsymbol{C}_0\boldsymbol{T}_V, \quad (26)$$

and the modal distributed voltage source $\boldsymbol{V}_{Fm}^{'}(z)=\boldsymbol{T}_V^{-1}\boldsymbol{V}_F^{'}(z)$.

Similarly, the nth-order perturbation equation (21) can be decoupled as follows:

$$\frac{d}{dz}\begin{bmatrix}\boldsymbol{V}_{m,n}^{s}(z)\\ \boldsymbol{I}_{m,n}(z)\end{bmatrix}+\begin{bmatrix}\boldsymbol{0} & j\omega\boldsymbol{L}_{m,0}\\ j\omega\boldsymbol{C}_{m,0} & \boldsymbol{0}\end{bmatrix}\begin{bmatrix}\boldsymbol{V}_{m,n}^{s}(z)\\ \boldsymbol{I}_{m,n}(z)\end{bmatrix}=\begin{bmatrix}\boldsymbol{V}_{Fm}^{n'}(z)\\ \boldsymbol{I}_{Fm}^{n'}(z)\end{bmatrix}, \quad (27)$$

where the nth-order modal scattering voltage $\boldsymbol{V}_{m,n}^{s}(z)$ and modal current $\boldsymbol{I}_{m,n}(z)$ can be obtained as follows:

$$\begin{bmatrix}\boldsymbol{V}_{m,n}^{s}(z)\\ \boldsymbol{I}_{m,n}(z)\end{bmatrix}=\begin{bmatrix}\boldsymbol{T}_V & \boldsymbol{0}\\ \boldsymbol{0} & \boldsymbol{T}_I\end{bmatrix}\begin{bmatrix}\boldsymbol{V}_{n}^{s}(z)\\ \boldsymbol{I}_{n}(z)\end{bmatrix}, \quad (28)$$

and the nth-order modal distributed voltage source $\boldsymbol{V}_{Fm}^{n'}(z)$ and current source $\boldsymbol{I}_{Fm}^{n'}(z)$ can be obtained as follows:

$$\begin{bmatrix}\boldsymbol{V}_{Fm}^{n'}(z)\\ \boldsymbol{I}_{Fm}^{n'}(z)\end{bmatrix}=\begin{bmatrix}\boldsymbol{T}_V^{-1} & \boldsymbol{0}\\ \boldsymbol{0} & \boldsymbol{T}_I^{-1}\end{bmatrix}\begin{bmatrix}\boldsymbol{V}_{F}^{n'}(z)\\ \boldsymbol{I}_{F}^{n'}(z)\end{bmatrix}. \quad (29)$$

E. Boundary condition

Proper boundary conditions should be imposed to obtain the solution of equations (25) and (27). Using Thevenin equivalents of line terminations, the boundary condition for equations (11) and (12) can be written as:

$$\begin{aligned}V_0^s(-L/2,\varepsilon)&=V^{ex}(-L/2,\varepsilon)-Z_L I_0(L/2,\varepsilon),\\ V_0^s(L/2,\varepsilon)&=V^{ex}(L/2,\varepsilon)+Z_R I_0(L/2,\varepsilon),\end{aligned} \quad (30a)$$

$$\begin{aligned}V_n^s(-L/2,\varepsilon)&=-Z_L I_n(-L/2,\varepsilon),\\ V_n^s(L/2,\varepsilon)&=Z_R I_n(L/2,\varepsilon).\end{aligned} \quad (30b)$$

Substituting equation (13a) into equations (30a) and (30b), and expanding the excitation voltage $\boldsymbol{V}^{ex}(z,\varepsilon)$ with the same polynomials, the 0th-order and nth-order perturbation random boundary condition in equations (30a) and (30b) can be expanded into equations (31a) and (31b), respectively:

$$\begin{aligned}\sum_{p=0}^{P_0}V_0^{s,p}(-L/2)\phi_p(\varepsilon)&=\sum_{p=0}^{P_0}V_p^{ex}(-L/2)\phi_p(\varepsilon)-Z_L\sum_{p=0}^{P_0}I_0^p(-L/2)\phi_p(\varepsilon),\\ \sum_{p=0}^{P_0}V_0^{s,p}(L/2)\phi_p(\varepsilon)&=\sum_{p=0}^{P_0}V_p^{ex}(L/2)\phi_p(\varepsilon)+Z_R\sum_{p=0}^{P_0}I_0^p(L/2)\phi_p(\varepsilon),\end{aligned} \quad (31a)$$

$$\begin{aligned}\sum_{p=0}^{P_n}V_n^{s,p}(-L/2)\phi_p(\varepsilon)&=-Z_L\sum_{p=0}^{P_n}I_n^p(-L/2)\phi_p(\varepsilon),\\ \sum_{p=0}^{P_n}V_n^{s,p}(L/2)\phi_p(\varepsilon)&=Z_R\sum_{p=0}^{P_n}I_n^p(L/2)\phi_p(\varepsilon).\end{aligned} \quad (31b)$$

Similarly, through a stochastic Galerkin method, projecting equations (31a) and (31b) to the Legendre orthogonal basis, the 0th-order and nth-order perturbation boundary conditions can be obtained as follows:

$$\begin{aligned}V_0^{s,m}(-L/2)&=V_m^{ex}(-L/2)-Z_L I_0^m(-L/2),\\ V_0^{s,m}(L/2)&=V_m^{ex}(L/2)+Z_R I_0^m(L/2),\end{aligned} \quad (32a)$$

$$\begin{aligned}V_n^{s,m}(-L/2)&=-Z_L I_n^m(-L/2),\\ V_n^{s,m}(L/2)&=Z_R I_n^m(L/2).\end{aligned} \quad (32b)$$

F. RNTL terminal solution

Given the boundary conditions, the general solution of the 0th-order and nth-order perturbation modal equation can be easily solved, and thus, the final terminal solution for the voltage (current) of RNTL can be obtained by substituting these modal terms into equations (24), (28), (13), (10), and (8). For brevity, the solution is omitted here.

G. DNTL terminal solution

For DNTL, namely $\delta_h=0$ and $H_1\neq H_2$ in case *c* and case *d*, the induced voltage can be obtained by only taking the (Nth, 0th)-order PD-PCE solution.

H. RUTL terminal solution

For RUTL, namely $\delta_h\neq 0$ and $H_1=H_2$ in case *c*, the terminal solution can be obtained by only taking the (0th, Pth)-order PD-PCE solution.

III. NUMERICAL RESULTS AND APPLICATIONS

In this section, numerical simulations were performed to validate the proposed (Nth, Pth)-order PD-PCE method for the RNTL above an ideal ground under plane-wave illumination. For all cases, the length of the TLs is $L=1$ m, the radius is $r_a=0.5$ mm, and terminal resistances are $Z_L=Z_R=50\ \Omega$. The amplitude of the electric field is $E_0=100$ V / m and the frequency band ranges from 5 MHz to 4 GHz. The frequency interval was set to 5 MHz. Without loss of generality, the incident angle was set as $\theta=\pi/3$, $\varphi=\pi/6$, and $\alpha=\pi/6$.

A. Deterministic response analysis

First, the deterministic response of a nonuniform TL under plane-wave illumination was analyzed to validate the proposed method. The parameters of the TLs are shown in Table 2, where DUTL is chosen for comparison. The UCS method [9], which divides the DNTL into 600 local uniform segments to ensure sufficient accuracy, was chosen for comparison.

Table 2: Geometrical parameters of transmission lines

Analyzing Scenarios		H_1 /mm	H_2 /mm	δ_h /mm
A.1	case *c*: DNTL	12	14	0
	Comparison case *c*: DUTL	12	12	0
A.2	case *d*: DNTL	10	12	0
	Comparison case *d*: DUTL	12	12	0

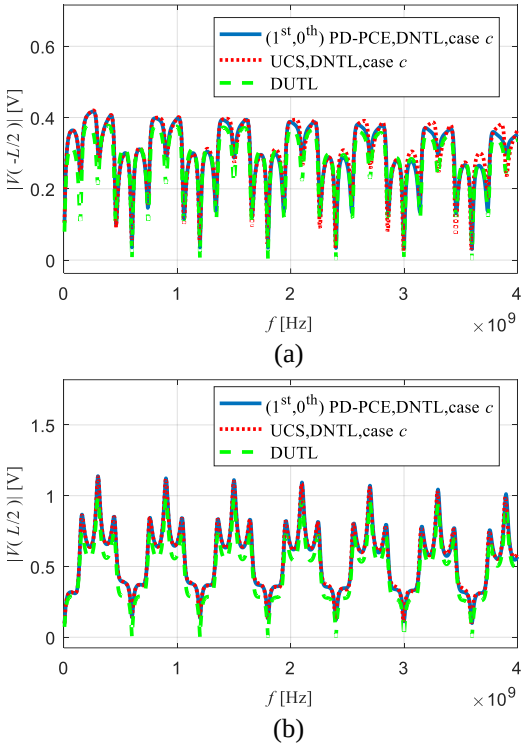

Fig. 3. Magnitude of induced voltage for DNTL of case *c* and the DUTL. (a) Induced voltage at the left end of the TL, and (b) induced voltage at the right end of TL.

A.1. DNTL of case *c*

Figures 3 (a) and (b) show the induced voltage at the left and right ends of the DNTL of case *c*, respectively. The blue curves are the results of the (1st, 0th)-order PD-PCE method. The dotted red curves are the results of the UCS method. It can be observed that at lower frequencies, the induced voltages derived from the PD-PCE method were consistent with those of UCS method at both ends of DNTL, whereas for frequencies above approximately 2 GHz, the induced voltage at the left end shows discrepancies for the two methods.

Figures 3 (a) and (b) also show the induced voltage (dashed green curves) at the left and right ends of the DUTL, respectively. For most frequencies, the induced voltage of the DNTL is larger than that of the DUTL.

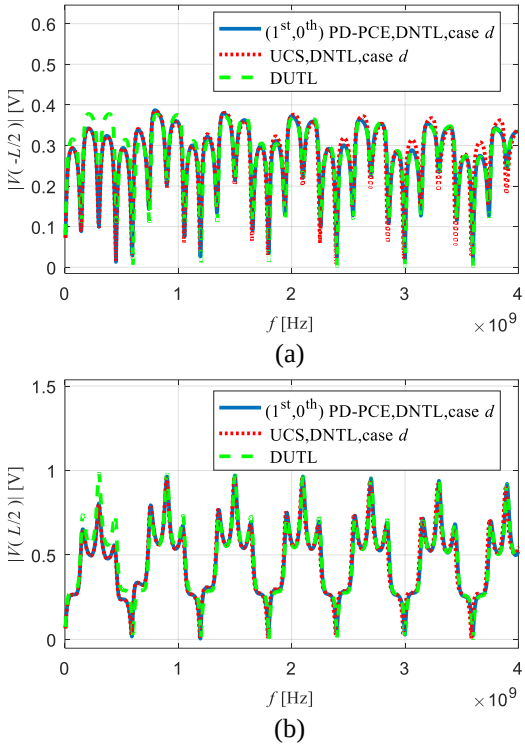

Fig. 4. Magnitude of induced voltage for the DNTL of case *d* and the DUTL. (a) Induced voltage at the left end of TL, and (b) induced voltage at the right end of TL.

A.2. DNTL of case *d*

Figures 4 (a) and (b) show the induced voltage at the left and right ends of the DNTL of case *d*, respectively. The blue curves are the results of the (1st, 0th)-order PD-PCE method for the DNTL. The dotted red curves are the results of the UCS method for the DNTL. Moreover, it can be observed that the induced voltage at the left end of the TL derived from the PD-PCE method is consistent with that derived from the UCS method at lower frequencies. However, for frequencies above approximately 2 GHz, the induced voltage at the left end shows discrepancies for the two methods. For the induced voltage at the right end of DNTL, at most frequency points, the results of the two methods are consistent with each other, which confirms the validity of the proposed method.

The induced voltage (dashed green curves) at the left and right ends of the DUTL is also shown in Figs. 4 (a) and (b), respectively. For most frequencies, the induced voltage of the DNTL is smaller than that of the DUTL, especially at lower frequencies.

Table 3 shows the comparison of computation time between the PD-PCE method and the UCS method. The simulations were performed on a workstation with an Intel Xeon CPU X5670 with clock frequency 2.93 GHz and 16 GB RAM. The (1st, 0th)-order PD-PCE method

takes approximately 9.9 s for 800 frequency points, whereas the UCS method takes approximately 890.2 s for 800 frequency points. The proposed (1st, 0th)-order PD-PCE method is approximately 89.9 times faster than the UCS method while maintaining the same level of accuracy.

Table 3: CPU time of the (1st, 0th)-order PD-PCE method and UCS method

Method	Order	Simulation Time /s
UCS	--	890.2
PD-PCE	(1st, 0th)	9.9

Table 4: Parameters of the transmission line

Analyzing Scenarios		H_1 /mm	H_2 /mm	δ_h /mm
B.1	case *a*	10	--	2
	Comparison case *a*: DUTL	10	--	0
B.2	case *b*	8	10	1
	Comparison case *b*: DUTL	10	10	0
B.3	case *c*	10	12	2
	Comparison case *c*: RUTL	10	10	2
B.4	case *d*	8	10	2
	Comparison case *d*: RUTL	10	10	2

B. Statistical response analysis of RNTL

In this section, the validity of the proposed PD-PCE method was confirmed. The MC method was chosen for comparison, which required 1000 simulations to provide sufficient samplings. The four cases of RNTL shown in Fig. 1 were analyzed. For case *a* and case *b*, DUTL was chosen for comparison. For case *c* and case *d*, RUTL was chosen for comparison. The parameters of the lines are shown in Table 4.

B.1. Random nonuniform transmission line of case *a*

Figs. 5 (a) and (b) show the probability density function (pdf) of the magnitude of the induced voltage at the right end of the RNTL for case *a* at f = 800 MHz and f = 3.5 GHz, respectively. The red curves are the results of the (1st, 5th)-order PD-PCE method, and the blue cross curves are the results of the MC method. It can be observed that the results of the two methods are consistent with each other at f = 800 MHz. However, there are minor discrepancies between the two methods at f = 3.5 GHz. This may be because the electromagnetic response of the TL is more sensitive to the variance of geometrical parameters at high frequencies.

Figures 6 (a) and (b) show the mean value and variance of the induced voltage (blue curves) at the right end of the RNTL of case *a* derived using the (1st, 5th)-order PD-PCE method, respectively. For comparison, Fig. 6 (a) shows the induced voltage at the right end of the DUTL (green dotted curves). It can be observed that the mean value of induced voltage of the RNTL equals the voltage of the DUTL, whereas the variance of RNTL exhibits periodical fluctuation.

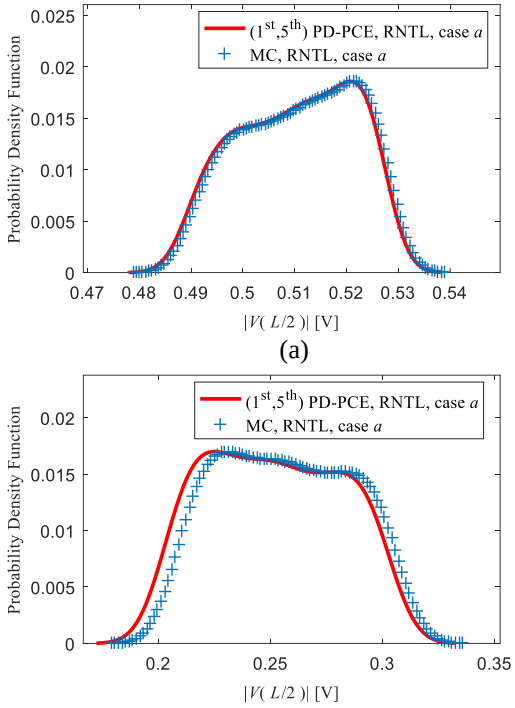

Fig. 5. Probability density function of induced voltage at the right end of the RNTL of case *a*: (a) f = 800 MHz, (b) f = 3.5 GHz.

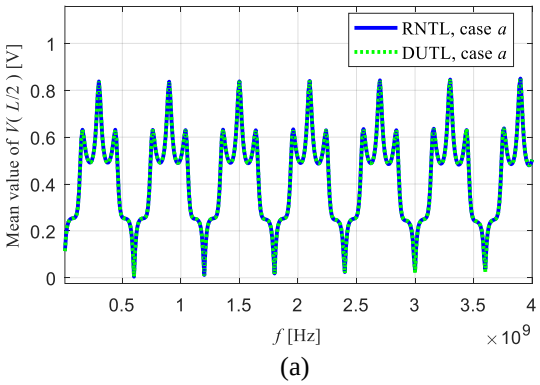

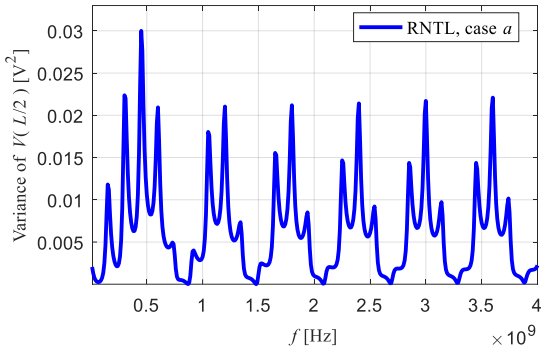

(b)

Fig. 6. (a) Induced voltage at the right end of the DUTL and mean value of induced voltage at the right end of the RNTL of case *a*. (b) Variance of the induced voltage at the right end of the RNTL of case *a*.

B.2. Random nonuniform transmission line of case b

Figures 7 (a) and (b) show the pdf of the magnitude of the induced voltage at the right end of the RNTL of case *b* at f = 800 MHz and f = 3.5 GHz, respectively. The red curves are the results of the (1st, 5th)-order PD-PCE method, and the blue cross curves are the results of the MC method. It can be observed that the results of the two methods are consistent with each other.

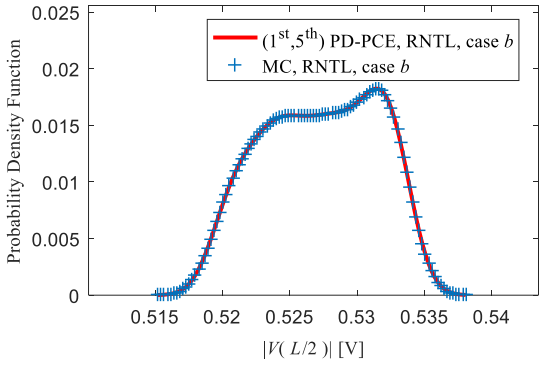

(a)

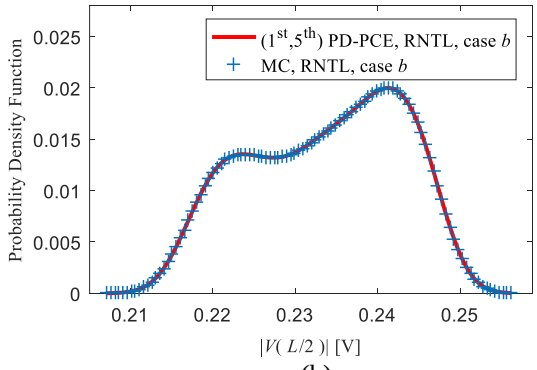

(b)

Fig. 7. Probability density function of induced voltage at the right end of the RNTL of case *b*: (a) f = 800 MHz, (b) f = 3.5 GHz.

Figures 8 (a) and (b) show the mean value and variance of induced voltage at the right end of the RNTL of case *b* obtained from the (1st, 5th)-order PD-PCE method. Figure 8 (a) also shows the induced voltage at the right end of the DUTL. It can be observed that the mean value of voltage of the RNTL deviates from the voltage of the DUTL at lower frequencies, whereas the variance of the RNTL shows strong periodical fluctuation.

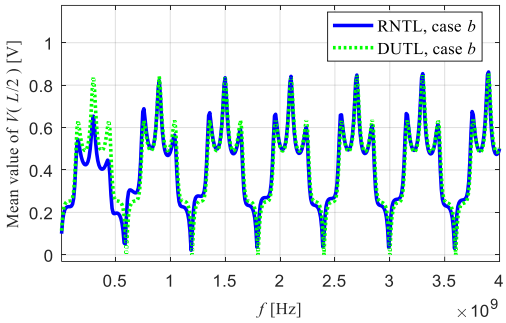

(a)

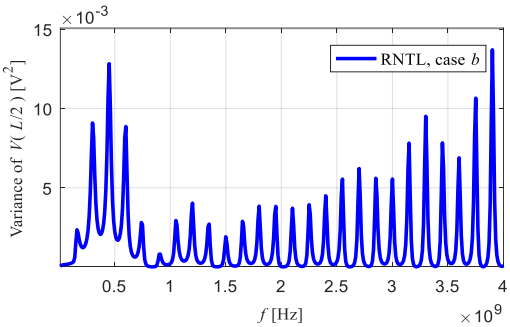

(b)

Fig. 8. (a) Induced voltage at the right end of the DUTL and the mean value of induced voltage at the right end of the RNTL of case *b*. (b) Variance of the induced voltage at the right end of the RNTL of case *b*.

B.3. Random nonuniform transmission line of case *c*

Figures 9 (a) and (b) show the pdf of induced voltage at the right end of the RNTL and RUTL of case *c* at f = 800 MHz and f = 3.5 GHz, respectively. It can be observed that, at f=800 MHz, the results of the two methods for both cases are consistent with each other, whereas at f = 3.5 GHz, there is a slight deviation between the results of the proposed PD-PCE method and the MC method. It can also be observed that the pdf of induced voltage of the RNTL is similar to that of the RUTL except with a different mean value.

Figures 10 (a) and (b) show the mean value and variance of induced voltage at the right end of the RNTL and RUTL of case *c* derived from the (1st, 5th)-order PD-PCE method, respectively. It can be observed that the mean value of voltage of the RNTL was larger than that of the RUTL at some frequency points, whereas the variance was almost the same.

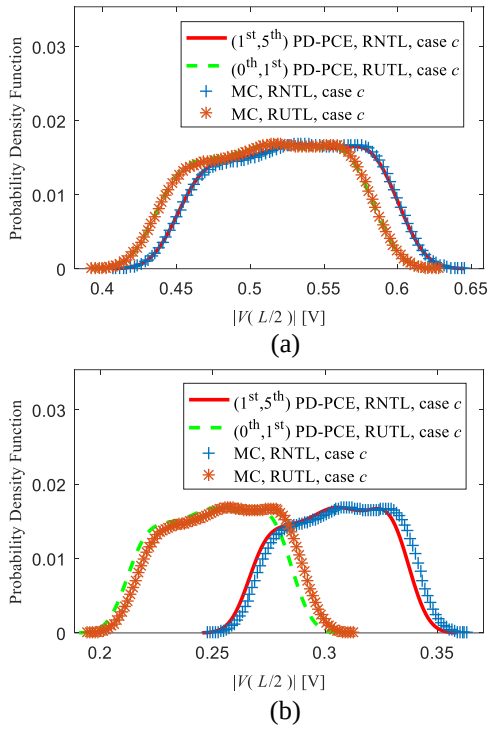

Fig. 9. Probability density function of induced voltage at the right end of RNTL and RUTL of case *c*: (a) f = 800 MHz, (b) f = 3.5 GHz.

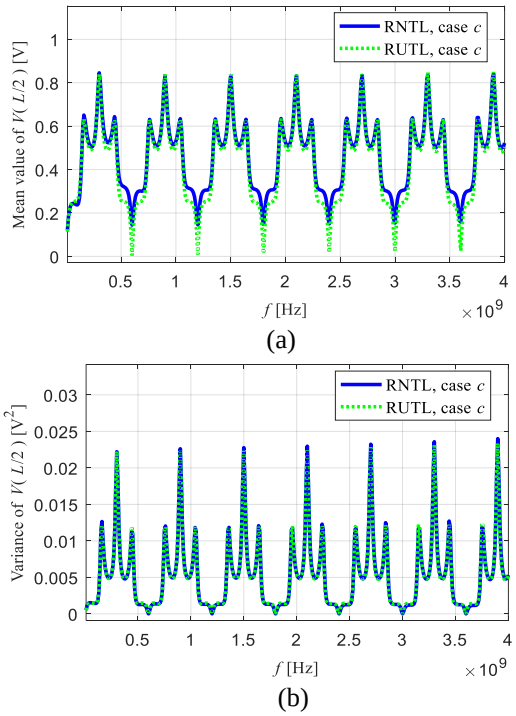

Fig. 10. (a) Mean value of induced voltage at the right end of the RNTL and RUTL of case *c*. (b) Variance of induced voltage at the right end of the RNTL and RUTL of case *c*.

B.4 Random nonuniform transmission line of case *d*

Figures 11 (*a*) and (*b*) show the pdf of induced voltage at the right end of the RNTL and RUTL of case *d* at f = 800 MHz and f = 3.5 GHz, respectively. The results derived from the proposed PD-PCE method and the MC method were consistent with each other at f = 800 MHz, whereas the results of the two methods show a slight deviation at f = 3.5 GHz. It can also be observed that the pdfs of the RNTL and RUTL were almost the same.

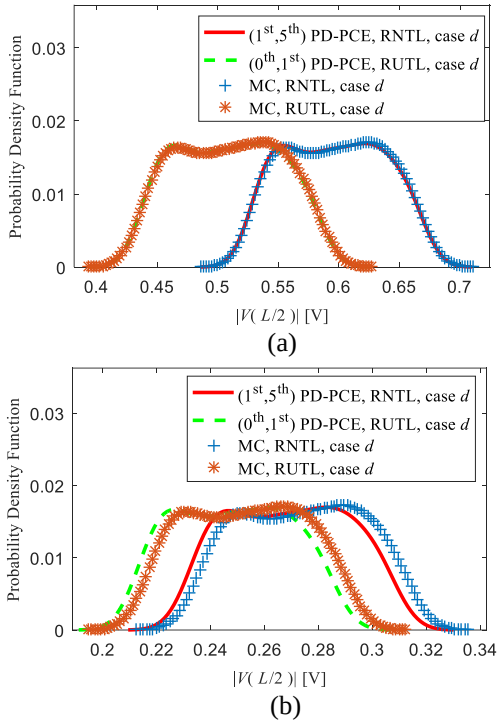

Fig. 11. Probability density function of induced voltage at the right end of the RNTL and RUTL: (a) f = 800 MHz, and (b) f = 3.5 GHz.

Figures 12 (*a*) and (*b*) show the mean value and variance of induced voltage at the right end of the RNTL and RUTL of case *d*, respectively. It can be observed that the mean value of voltage of the RNTL was slightly larger than that of the RUTL, whereas the variance was almost the same.

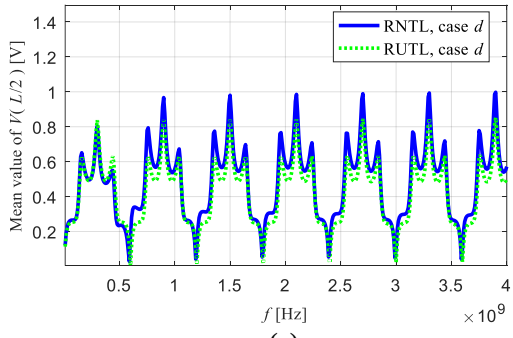

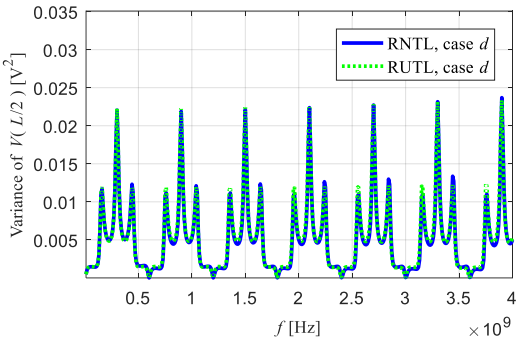

(b)

Fig. 12. (a) Mean value of induced voltage at the right end of the RNTL and RUTL of case *d*. (b) Variance of induced voltage at the right end of the RNTL and RUTL of case *d*.

Table 5 presents the computation time of the proposed (1st, 5th)-order PD-PCE method and MC method. The (1st, 5th)-order PD-PCE method takes approximately 9.8+6.8=16.6 s for 800 frequency points, whereas the MC method takes approximately 2.1*1000=2100 s for 800 frequency points. The proposed (1st, 5th)-order PD-PCE method is approximately 126.5 times faster than the MC method without losing accuracy.

Table 5: CPU time of (1st, 5th)-order PD-PCE method and MC method

Method	PCE Projection/s	Total Time/s	Repeat Time
MC	0	2.1*1000	1000
PD-PCE	9.8	6.8	2+6

IV. CONCLUSION

In this paper, an (N^{th}, P^{th})-order PD-PCE method for the analysis of random nonuniform transmission line response under plane-wave illumination is presented. Simulation results show that the PD-PCE method is accurate and computationally efficient compared with the UCS and MC methods. Under the assumption of weak level of nonuniformity, small number of random variables, and lower frequency band, this method is effective and can provide quantitative guidance for evaluating the effects of the nonuniformity and uncertainty of transmission lines on the reliability of electrical systems.

REFERENCES

[1] S. Barmada, A. Musolino, and M. Raugi, "Response bounds analysis for transmission lines characterized by uncertain parameters," *Applied Comput. Electromagn. Society J.*, vol. 20, no. 3, pp. 213-220, Jan. 2005.

[2] G. Zhang, J. J. Bai, L. X. Wang, and X. Y. Peng, "Stochastic analysis of multi-conductor cables with uncertain boundary conditions," *Applied Comput. Electromagn. Society J.*, vol. 33, no. 8, pp. 847-853, Aug. 2018.

[3] M. Cernobryvko, D. V. Ginste, and D. D. Zutter, "A two-step perturbation technique for nonuniform single and differential lines," *IEEE Trans. on Microw. Theory and Tech.*, vol. 61, no. 5 pp. 1758-1767, May 2013.

[4] P. Manfredi, D. V. Ginste, and D. D. Zutter, "An effective modeling framework for the analysis of interconnects subject to line-edge roughness," *IEEE Microw. Wirel. Co.*, vol. 25, no. 8, pp. 502-504, Aug. 2015.

[5] P. Manfredi, D. D. Zutter, and D. V. Ginste, "Analysis of nonuniform transmission lines with an iterative and adaptive perturbation technique," *IEEE Trans. on Electromagn. Compat.*, vol. 58, no. 3, pp. 859-867, Apr. 2016.

[6] F. Grassi, P. Manfredi, and X. Liu, "Effects of undesired asymmetries and nonuniformities in differential lines," *IEEE Trans. on Electromagn. Compat.*, vol. 59, no. 5, pp. 1613-1624, Oct. 2017.

[7] I. Jacek, "Equivalent circuits for nonuniform transmission line simulation," *Applied Comput. Electromagn. Society J.*, vol. 25, no. 9, pp. 764-779, Sep. 2010.

[8] Y. Sun and X. Wang, "Novel extraction method of inductance parameter for nonuniform transmission line in anisotropic dielectric," *Applied Comput. Electromagn. Society J.*, vol. 32, no. 1, pp. 15-23, Jan. 2017.

[9] C. R. Paul, *Analysis of Multiconductor Transmission Lines*, New York: John Wiley and Sons, 1994.

[10] F. A. Rachidi, "A review of field-to-transmission line coupling models with special emphasis to lightning-induced voltages on overhead lines," *IEEE Trans. on Electromagn. Compat.*, vol. 54, no. 4, pp. 898-911, Aug. 2012.

[11] C. A. Nucci, F. Rachidi, and M. Rubinstein, "An overview of field-to-transmission line interaction," *Applied Comput. Electromagn. Society N.*, vol. 22, no. 1, pp. 9-27, Jan. 2007.

[12] C. P. Robert and G. Casella, *Introducing Monte Carlo Methods with R*, New York, Springer, 2009.

[13] Q. Zhang, J. J. Liu, J. McMacken, J. Thomson, and P. Layman, "Development of robust interconnect model based on design of experiments and multi objective optimization," *IEEE Trans. on Electron. Devices*, vol. 48, no. 9, pp. 1885-1891, Sep. 2001.

[14] I. S. Stievano, P. Manfredi, and F. G. Canavero, "Stochastic analysis of multiconductor cables and interconnects," *IEEE Trans. on Electromagn. Compat.*, vol. 53, no. 2, pp. 501-507, May 2011.

[15] P. Manfredi and F. G. Canavero, "Polynomial chaos for random field coupling to transmission lines," *IEEE Trans. on Electromagn. Compat.*, vol.54, no. 3, pp. 677-680, June 2012.
[16] O. J. Alkhateeb and N. Ida, "Data-driven arbitrary polynomial chaos for uncertainty quantification in filters," *Applied Comput. Electromagn. Society J.*, vol.33, no. 9, pp. 1048-1051, Sep. 2018.
[17] E. N. Protonotarios and O. Wing, "Analysis and intrinsic properties of the general nonuniform transmission line," *IEEE Trans. Microw. Theory Tech.*, vol. 15, no. 3, pp. 142-150, Mar. 1967.
[18] J. F. Mao and Z. F. Li, "Analysis of the time response of nonuniform multiconductor transmission lines with a method of equivalent uniform cascaded section network chain," *IEEE Trans. Microw. Theory Tech.*, vol. 40, no. 5, pp. 948-954, May 1992.
[19] P. Gómez, P. Moreno, and J. L. Naredo, "Frequency-domain transient analysis of nonuniform lines with incident field excitation," *IEEE Trans. Power Del.*, vol. 20, no. 3, pp. 2273-2280, Jul. 2005.
[20] M. A. Khalaj, "Analysis of coupled or single nonuniform transmission lines using step-by-step numerical integration," *Prog. Electromagn. Res.*, vol. 58, pp. 187-198, 2006.
[21] C. Jullien, P. Besnier, M. Dunand, and I. Junqua, "Advanced modeling of crosstalk between an unshielded twisted pair cable and an unshielded wire above a ground plane," *IEEE Trans. Power Del.*, vol. 55, no. 1, pp. 183-194, Feb. 2013.
[22] M. A. Khalaj, "Analysis of nonuniform transmission lines using the equivalent sources," *Prog. Electromagn. Res.*, vol. 71, pp. 95-107, 2007.

Jinpeng Yang received the B.S. degree from Jilin University in 2013. He is currently working toward the Ph.D. degree at Jilin University. His research interests include transmission line modeling and statistical electromagnetics.

Xiaoying Sun received the B.S. and M.S. degrees from Jilin University, Jilin, China, in 1991 and 1994, respectively, and the Ph.D. degree in Communication and Information System from Jilin University, where he is currently a Professor with the Laboratory of Signals Detection and Processing. He is currently Professor, Changbai Mountain scholar, Dean of the Communication Engineering College, Jilin University. His current research interests include vehicle electromagnetic compatibility, array signal processing and passive sources localization.

Yu Zhao received the B.S. degree from North-east Normal University, and M.S. degree from Jilin University, China, in 1993 and 1996, respectively, and the Ph.D. degree in Communication and Information System from Jilin University in 2005. She is currently an Associate Professor of Jilin University. Her current research interest is electromagnetic compatibility.

Jian Chen received the Ph.D. degree in Communication and Information systems from Jilin University, Changchun, China, in 2007. From February 2014 to February 2015, he was a Visiting Scholar with the School of Electric and Electrical Engineering, Leeds University, Leeds, UK. He is currently an Associate Professor with the College of Communication Engineering, Jilin University, Changchun, China. His research interests include array signal processing, electromagnetic compatibility.

Hanqing Wang received the B.S. degree in Communication Engineering from Jilin University in 2016. He is currently working toward the master's degree in Communication and Information System. His current research interest is vehicle EMC.